Lab on a Chip

PAPER

View Article Online
View Journal

Cite this: DOI: 10.1039/c7lc00327g

Biocompatible and label-free separation of cancer cells from cell culture lines from white blood cells in ferrofluids†

Wujun Zhao,[a] Rui Cheng,[b] So Hyun Lim,[c] Joshua R. Miller,[a] Weizhong Zhang,[a] Wei Tang,[a] Jin Xie[a] and Leidong Mao*[b]

This paper reports a biocompatible and label-free cell separation method using ferrofluids that can separate a variety of low-concentration cancer cells from cell culture lines (~100 cancer cells per mL) from undiluted white blood cells, with a throughput of 1.2 mL h^{-1} and an average separation efficiency of 82.2%. The separation is based on the size difference of the cancer cells and white blood cells, and is conducted in a custom-made biocompatible ferrofluid that retains not only excellent short-term viabilities but also normal proliferations of 7 commonly used cancer cell lines. A microfluidic device is designed and optimized specifically to shorten the time of live cells' exposure to ferrofluids from hours to seconds, by eliminating time-consuming off-chip sample preparation and extraction steps and integrating them on-chip to achieve a one-step process. As a proof-of-concept demonstration, a ferrofluid with 0.26% volume fraction was used in this microfluidic device to separate spiked cancer cells from cell lines at a concentration of ~100 cells per mL from white blood cells with a throughput of 1.2 mL h^{-1}. The separation efficiencies were 80 ± 3%, 81 ± 5%, 82 ± 5%, 82 ± 4%, and 86 ± 6% for A549 lung cancer, H1299 lung cancer, MCF-7 breast cancer, MDA-MB-231 breast cancer, and PC-3 prostate cancer cell lines, respectively. The separated cancer cells' purity was between 25.3% and 28.8%. In addition, the separated cancer cells from this strategy showed an average short-term viability of 94.4 ± 1.3%, and these separated cells were cultured and demonstrated normal proliferation to confluence even after the separation process. Owing to its excellent biocompatibility and label-free operation and its ability to recover low concentrations of cancer cells from white blood cells, this method could lead to a promising tool for rare cell separation.

Received 27th March 2017,
Accepted 29th May 2017

DOI: 10.1039/c7lc00327g

rsc.li/loc

Introduction

Microfluidic manipulation of cells in magnetic liquids,[1] *i.e.*, negative magnetophoresis, has led to a number of recent applications in cell separation,[1–4] trapping and focusing,[5–8] and density measurements.[9–13] Its working principle is as follows: cells without any labels placed inside uniformly magnetic media – magnetic liquids – act as "magnetic holes".[14] A magnetic field gradient attracts the magnetic media, which causes the "magnetic holes" – cells – to be preferentially pushed away. This way, cells can be continuously manipulated in a label-free fashion. The magnetic force acting on the cells is proportional to their sizes,[1,15] very similar to buoyancy force, which allows for size-based manipulation. Typical devices for conducting "negative magnetophoresis" assays are simple and low-cost, involving only channels and permanent magnets. Their operation does not necessitate accessories such as power supplies or function generators. Because of its label-free, low-cost and simple-to-use nature, "negative magnetophoresis" has been used recently for cell manipulation. For example, Demirci's group developed a static-flow system in the form of magnetic liquids – paramagnetic salt solutions – to precisely measure subtle density differences among cell groups.[9,10] Salt solutions containing transition and lanthanide metals, such as Mn^{2+} or Gd^{3+}, are weakly magnetic due to their unpaired inner-shell electrons that produce a magnetic moment. Our group demonstrated continuous-flow ferrohydrodynamic separation of HeLa cells from whole blood in another form of magnetic liquids – ferrofluids.[16] Ferrofluids are colloidal suspensions of magnetic nanoparticles with diameters of approximately 10 nm. Although both paramagnetic salt solutions and ferrofluids have served as media in "negative magnetophoresis" assays, ferrofluids were considered to be better suited for applications such as high-throughput separation that requires a continuous flow,

[a] Department of Chemistry, University of Georgia, Athens, Georgia 30602, USA
[b] College of Engineering, University of Georgia, Athens, Georgia 30602, USA. E-mail: mao@uga.edu
[c] Department of Microbiology, University of Georgia, Athens, Georgia 30602, USA

† Electronic supplementary information (ESI) available. See DOI: 10.1039/c7lc00327g

because of their stronger magnetic properties, while paramagnetic salt solutions exceled in static-flow applications such as density measurement.

Cell separation based on "negative magnetophoresis" in ferrofluids is facing its own challenges, especially in rare cell separation where cell integrity needs to be maintained for further analysis, while typically less than 1000 cells in one milliliter of sample are available and need to be enriched in a high-throughput and high-efficiency manner.[17] The challenges associated with cell separation in ferrofluids are three-fold. First of all, ferrofluids are not natural media for cells; they need to be rendered biocompatible so that cells remain alive and their normal functions are kept intact during and after the separation for post-separation analysis. This is not trivial; although progress was made recently through preserving the viability and normal proliferation of cells in custom-made ferrofluids,[3,18] the biocompatibility of ferrofluids remains to be a significant challenge for cell separation applications. For example, although Yellen's group developed a bovine serum albumin (BSA)-coated ferrofluid in which human umbilical vein endothelial cells (HUVEC) had more than 95% viability after 2 hours of exposure and were able to maintain normal proliferation afterwards,[18] this ferrofluid was only used under static-flow conditions for relatively slow cell manipulation, and its colloidal stability could be an issue in high-throughput and continuous-flow cell separation applications, because of the thick BSA surfactant layer used for particle functionalization. Although Koser's group reported a citrate-stabilized ferrofluid and demonstrated a 75% viability of blood cells after several hours of exposure to it,[3] a long-term cell proliferation study using this ferrofluid was not conducted. In summary, only a very limited number of cells were studied in these custom-made ferrofluids under operation conditions that were not always compatible for continuous-flow cell separation, and data didn't often provide both short-term and long-term impacts on them after separation. As a result, there is an urgent need for a new ferrofluid that can minimize its negative effects on mammalian cells and, at the same time, is colloidally stable for high-throughput and continuous-flow operation under strong magnetic fields. The second challenge comes from device design for cell separation in ferrofluids. Even with a biocompatible ferrofluid, it is still necessary to reduce the time of cells' exposure to it down to an absolute minimum, because prolonged exposure time will inevitably lead to particle endocytosis and/or diffusion and affect cell viability and normal functions.[19] For example, we observed in this study that long exposure of A549 lung cancer cells to ferrofluids resulted in higher cellular uptake of nanoparticles and slower cell growth. In previous publications, the majority of time of cells' exposure to ferrofluids came from sample preparation and sample extraction that could last up to hours.[3,16,20] As a result, a new one-step device design that integrates sample preparation and extraction on-chip could significantly reduce exposure time and improve overall biocompatibility of the assay. The third challenge is associated with the low concentration of target cells in rare cell separation. In order to capture a meaningful number of target cells, throughput of at least 1 mL h^{-1} and separation efficiency of at least 80% under low concentration (<1000 cells per mL) conditions are necessary.[21] Although cell separation in ferrofluids was demonstrated before, it mostly focused on the separation of bacteria and yeast cells,[4,20] bacteria and red blood cells,[3] and HeLa cells and mouse blood.[16] The throughputs of these studies were relatively low, and the target cells were at a much higher concentration (*e.g.*, 10^5–10^6 cells per mL) than the definition of rare cells. It is therefore necessary to systematically optimize the device and ferrofluid design so that the throughput and efficiency of separation are comparable to those needed for rare cell separation.

In this study, we addressed the above-mentioned three challenges associated with rare cell separation in ferrofluids, by demonstrating label-free separation of low-concentration cancer cells from cell culture lines at a concentration of ~100 cancer cells per mL from undiluted white blood cells at a concentration of ~10^6 cells per mL in a newly developed biocompatible ferrofluid, with an optimized device design that achieved a throughput of 1.2 mL h^{-1} and a separation efficiency of greater than 80%. Cells were only exposed to ferrofluids for seconds in this process. We first developed a new water-based ferrofluid in which 7 commonly used cancer cell lines showed excellent short-term viability and normal proliferation to confluence after extended exposure. The ferrofluid possessed ideal properties, including its pH value, tonicity, materials and surfactants of nanoparticles, as a biocompatible medium for mammalian cells, while at the same time the overall colloidal stability of this ferrofluid was well maintained to allow for high-throughput and continuous-flow separation under strong magnetic fields. We further developed a new device design that significantly reduces the time of cells' exposure to ferrofluids, from hours to seconds, by taking advantage of the laminar flow nature of liquids in microchannels.[22,23] The design is explained in detail in Fig. 1. Briefly, in a frequently used setup for ferrohydrodynamic cell separation,[3,4,16,20] the majority of ferrofluid exposure time came from sample preparation (*e.g.*, off-chip premixing between ferrofluids and cells) and sample extraction (*e.g.*, off-chip washing of cells after separation), as shown in Fig. 1a and b. However, the only time that cells needed to be exposed to ferrofluids was when they were actually being separated from each other. As a result, a device design that incorporates both on-chip sample preparation and extraction could significantly reduce exposure time and improve overall biocompatibility of the assay. In this device design, cell samples, ferrofluids, and a buffer were injected into a main channel through individual inlets, as shown in Fig. 1c. When they combined in the main channel, cell samples mixed with the ferrofluid almost instantaneously because of strong magnetic convection,[24,25] and then were separated based on their size difference. Large cells moved across the ferrofluid layer with

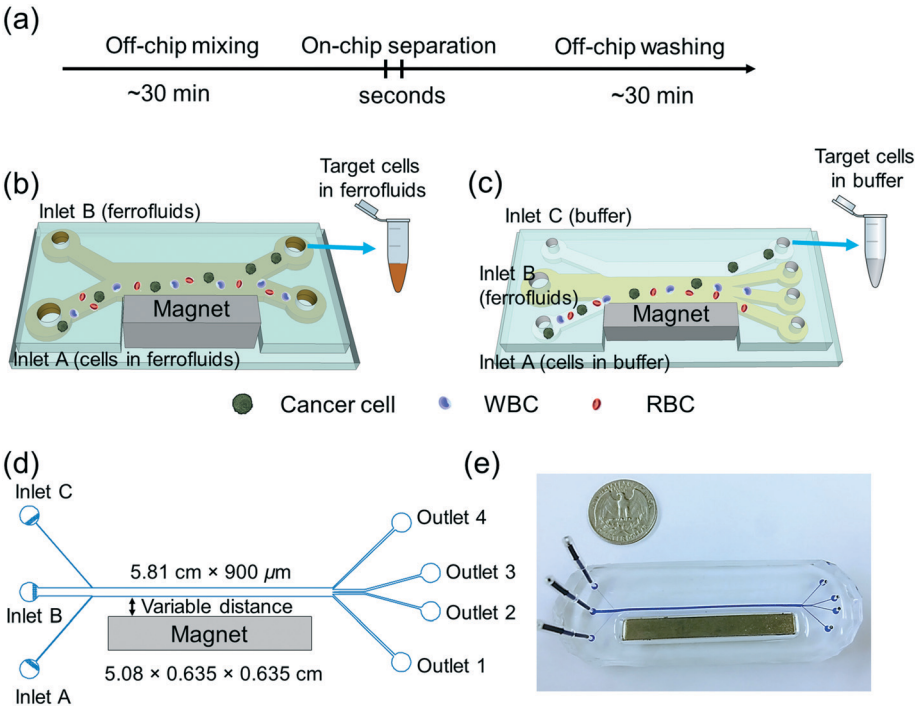

Fig. 1 (a) Processing time of existing cell separation in ferrofluids involves time-consuming pre-mixing of cells with ferrofluids (~30 minutes) and off-chip washing steps (~30 minutes), while separation takes place within seconds. The total time of cells' exposure to ferrofluids is estimated to be 1–2 hours. (b) Schematic illustration of an existing cell separation device. Cell mixtures are mixed with ferrofluids before separation and target cells are still in contact with ferrofluids after separation. (c) Schematic illustration of the proposed biocompatible cell separation in ferrofluids. The cell sample, ferrofluid, and buffer are injected into the device without pre-mixing. Cells are only in contact with ferrofluids when they are separated from each other. After separation, larger cancer cells are extracted into the buffer stream, eliminating the washing step. The total time of cells' exposure to ferrofluids is estimated to be seconds. (d) Top-view of the proposed device, which consists of a microchannel and a permanent magnet, their relevant dimensions, and labeling of inlets and outlets. (e) A photo of the prototype device with a U.S. quarter for size comparison. Blue dye is used to visualize the channel.

a faster velocity than smaller ones. Towards the end of the channel, larger cells reached the ferrofluid/buffer boundary and were extracted into the buffer stream containing an extremely low concentration of nanoparticles diffused from the ferrofluid stream. This way, cells were only exposed to ferrofluids when necessary (*i.e.*, separation) and the exposure time was determined by the flow rate and channel length, which in this design was on the order of seconds. Finally, we performed a systematic parametric study of key factors influencing the performance of this separation method, and determined parameters for high-throughput and high-efficiency low-concentration cancer cell separation of cell culture lines from undiluted white blood cells.

Experimental section

Synthesis and characterization of biocompatible ferrofluids

Ammonium hydroxide solution (NH_4OH, 28% w/w), iron(II) chloride tetrahydrate ($FeCl_2{\cdot}4H_2O$), iron(III) chloride hexahydrate ($FeCl_3{\cdot}6H_2O$), nitric acid (HNO_3), iron(III) nitrate nonahydrate ($Fe(NO_3)_3{\cdot}9H_2O$), and sodium hydroxide (NaOH) were purchased from a commercial vendor (Sigma-Aldrich, St. Louis, MO). All reagents were used as-received. Maghemite nanoparticles were synthesized by a chemical co-precipitation method.[16,26] In a typical reaction, 50 mL of ammonium hydroxide solution was quickly added to a mixture of 100 mL of 0.4 M iron(II) chloride tetrahydrate and 0.8 M iron(III) chloride hexahydrate, followed by stirring at room temperature for 30 minutes. The suspension was then centrifuged at 2000 × *g* for 3 minutes and the precipitate was dispersed in 200 mL of 2 M nitric acid and 0.35 M iron(III) nitrate nonahydrate. The mixture was maintained at 90 °C for 1 hour. During this time, the color of the mixture changed from black (Fe_3O_4) to reddish brown (Fe_2O_3). The maghemite nanoparticle suspension was centrifuged at 3000 × *g* for 3 minutes and finally dispersed in 120 mL of deionized (DI) water, yielding a stable dispersion with a pH of 1.5–2. The pH of the dispersion was adjusted to 2.9 using 1 M sodium hydroxide solution. 40 mL of Atlox 4913 (Croda, Inc., Edison, NJ), a graft copolymer solution, was added to the dispersion and stirred for 5 minutes before raising the pH to 7.0. The dispersion was then vigorously stirred at room temperature for 1 hour and the resulting ferrofluid was dialyzed with a dialysis membrane (Spectrum Labs Inc., Rancho Dominguez, CA) against DI water for one week. DI water was refreshed every 24 hours. After dialysis, excess water was vaporized at 72 °C. Finally, 10% (v/v) 10× Hanks' balanced salt solution (HBSS; Life Technologies, Carlsbad, CA) was added to the ferrofluid to render it

isotonic for cells, followed by adjusting the pH to 7.0. Sterile filtration of the ferrofluid was performed with a 0.2 μm filter (VWR, Radnor, PA) and the ferrofluid was exposed to UV light for 12 hours before experimental use.

The size and morphology of maghemite nanoparticles were characterized *via* transmission electron microscopy (TEM; FEI Corp., Eindhoven, the Netherlands). The magnetic properties of the ferrofluid were measured at room temperature using a vibrating sample magnetometer (VSM; MicroSense, LLC, Lowell, MA) with a 2.15 T electromagnet. The magnetic moment of the ferrofluid was measured over a range of applied fields from −21.5 to +21.5 kOe. The measurements were conducted in step field mode at a step size of 250 Oe s^{-1}. The zeta potential of the ferrofluid was measured with a Zetasizer Nano ZS (Malvern Instruments Inc., Westborough, MA).

Cell cultures and sample preparation

7 cancer cell lines (ATCC, Manassas, VA) including two lung cancer cell lines (A549 and H1299), three breast cancer cell lines (HCC1806, MDA-MD-231 and MCF-7), one cervical cancer cell line (HeLa), and one prostate cancer cell line (PC-3) were used to characterize the biocompatibility of the ferrofluid. A549, H1299, HCC1806, and PC-3 cells were cultured in RPMI-1640 medium (Mediatech, Inc., Manassas, VA) supplemented with 10% (v/v) fetal bovine serum (FBS; Life Technologies, Carlsbad, CA) and 1% (v/v) penicillin/streptomycin solution (Mediatech, Inc., Manassas, VA) at 37 °C under a humidified atmosphere of 5% CO_2. HeLa cells were cultured in Dulbecco's modified Eagle's medium (DMEM; Life Technologies, Carlsbad, CA) supplemented with 10% (v/v) FBS and 1% (v/v) penicillin/streptomycin solution at 37 °C under a humidified atmosphere of 5% CO_2. MDA-MB-231 and MCF-7 cells were cultured in DMEM supplemented with 10% (v/v) FBS, 1% (v/v) penicillin/streptomycin solution and 0.1 mM non-essential amino acid (NEAA; Life Technologies, Carlsbad, CA). All cell lines were released through incubation with 0.05% trypsin–EDTA solution (Life Technologies, Carlsbad, CA) at 37 °C for 5–10 minutes.

A549, H1299, MCF-7, MDA-MB-231, and PC-3 cells were used not only in the ferrofluid's biocompatibility characterization but also in cell separation experiments. Therefore, these five cell lines were stained with 2 μM CellTracker Green (Life Technologies, Carlsbad, CA) at 37 °C for 30 minutes before separation. The resulting cell suspensions were then centrifuged at 200 × *g* for 5 minutes and suspended in phosphate buffered saline (PBS; Life Technologies, Carlsbad, CA) with 2% (v/v) FBS before use. For a validation experiment of the simulation of separation of cancer cells from cell culture lines and red blood cells (RBCs), human whole blood (Streck, Omaha, NE) was diluted 1000 times with PBS to achieve a concentration of 2×10^6 cells per mL. For separation of low-concentration cancer cells from cell culture lines from undiluted white blood cells (WBCs), WBCs were obtained from undiluted human whole blood (Zen-Bio, Research Triangle Park, NC) with its RBCs lysed by RBC lysis buffer (eBioscience, San Diego, CA). The concentration of WBCs was on the order of 10^6 cells per mL. 100 cancer cells pre-stained with CellTracker Green were spiked into 1 mL of either diluted whole blood or undiluted WBCs. Cancer cells were first counted with a hemacytometer (Hausser Scientific, Horsham, PA) and serially diluted in culture medium to achieve a solution with approximately 1×10^4 cells per mL. Cells were then counted with a Nageotte counting chamber (Hausser Scientific, Horsham, PA) to determine the number of cells per μL. 100 cells (~10 μL) were spiked into 1 mL of WBCs. The number of cells spiked was determined by the average of two counts, with less than 5% difference between the counts.

Characterization of cell biocompatibility after exposure to ferrofluids

Cell viability was evaluated by 3-(4,5-dimethylthiazol-2-yl)-2,5-diphenyltetrazolium bromide (MTT) assay. A549 cells were first incubated in each well of a 96-well plate (Corning Inc., Corning, NY) for a total of 24 hours. Ferrofluids of varying concentrations (0.05%, 0.19%, 0.22%, and 0.26% v/v) were added into the plate. After incubation for 12 hours, the ferrofluid and medium were removed and cells were washed three times with PBS. MTT (ATCC, Manassas, VA) assay was then performed to determine the cell viability following the manufacturer's recommended protocol. The cell viability of the other 6 cell lines was investigated by the same MTT assay with a 0.26% (v/v) ferrofluid after 2 hours of incubation.

The cell proliferation rate was also assessed by MTT assay. A549 cells were first incubated with ferrofluids (0.26% v/v) for 1 minute and 2 hours, respectively, at 37 °C under a humidified atmosphere of 5% CO_2. Cells were then washed three times with PBS and released through incubation with 0.05% trypsin–EDTA solution. 4000 cells were seeded in each well of a 96-well plate. MTT assay was performed every 24 hours to determine the growth rate following the manufacturer's recommended protocol. The medium was changed on the third day. The proliferation of the other 6 cancer cell lines was investigated by attempting to culture cells to confluence after exposing them to ferrofluids for 2 hours.

Characterization of cell biocompatibility after cell separation experiments

Short-term viability after separation was examined using a Live/Dead assay (Life Technologies, Carlsbad, CA). 1×10^6 A549 cells were injected through inlet A at a flow rate of 20 μL min^{-1}. After separation, cells from outlet 4 were collected and incubated with a working solution (2 μM calcein-AM and 4 μM propidium iodide (PI)) for 30 minutes at room temperature. After the solution was removed and washed with PBS, the labeled cells were observed under a fluorescence microscope (Carl Zeiss, Inc., Germany) for counting. For long-term proliferation, the separated A549 cells were collected into a centrifuge tube and spun down to remove the buffer, and then the cells were suspended in complete culture medium

and seeded into a 24-well plate (Corning Inc., Corning, NY). The cells were then cultured at 37 °C under a humidified atmosphere of 5% CO_2, and the medium was refreshed every 24 h during the first 3 days. The cellular morphology was inspected every 24 hours.

Cellular nanoparticle uptake

A nanoparticle uptake study was conducted with A549 lung cancer cells. 1×10^5 A549 cells were seeded in each well of a 4-well chamber slide (Thermo Fisher Scientific, Waltham, MA). After 24 hours of incubation, ferrofluids were added and incubated with cells at 37 °C for 1 minute and 2 hours, respectively. The ferrofluids were then removed and the cells were washed three times with PBS. Next, the cells were fixed with ice-cold 95% ethanol (Thermo Fisher Scientific, Waltham, MA) for 15 minutes. Subsequently, the cells were incubated with Prussian blue staining solution (a mixture of equal volumes of 1.2 mM hydrochloric acid and 4% w/v potassium ferrocyanide solution; Sigma-Aldrich, St. Louis, MO) for 15 minutes at room temperature. The cells were then rinsed with DI water and counterstained with pararosaniline solution (Sigma-Aldrich, St. Louis, MO) for 10 minutes. After consecutive dehydrations with 70%, 90%, and 100% ethanol, the chamber was removed and the slide was mounted. The slide was then examined using a light microscope (Carl Zeiss, Inc., Germany).

Device fabrication and experimental setup

Microfluidic devices were made of polydimethylsiloxane (PDMS) using standard soft lithography techniques.[27] The thickness of the microfluidic channel was measured to be 52 μm using a profilometer (Veeco Instruments, Inc., Chadds Ford, PA). A NdFeB permanent magnet (K&J Magnetics, Inc., Pipersville, PA) was embedded into the PDMS channel with its magnetization direction vertical to the channel during the curing stage. The magnet is 5.08 cm in length and 0.635 cm in both width and thickness. The device and magnet dimensions are depicted in Fig. 1d, and a photo of the system is shown in Fig. 1e. The flux density at the center of the magnet's surface was measured to be 390 mT using a Gauss meter (Sypris, Orlando, FL) and an axial probe with 0.381 mm diameter of circular active area. The fabricated devices were flushed with 70% ethanol (Decon Labs, Inc., King of Prussia, PA) for 10 minutes before use. During a typical experiment, a microfluidic device was placed on the stage of an inverted microscope (Carl Zeiss, Inc., Germany) for observation and recording. Three fluids were controlled by individual syringe pumps (Chemyx, Inc., Stafford, TX) with tunable flow rates. Cell samples, ferrofluids, and PBS containing 2% (v/v) FBS were injected into the device through different inlets. Images and videos of microparticles and cells were recorded with a high-resolution CCD camera (Carl Zeiss, Inc., Germany).

Polystyrene microparticles (Polysciences, Inc., Warminster, PA) with diameters of 15.7 μm and 5.8 μm were prepared in PBS at a concentration of 2×10^6 particles per mL for device calibration. Microparticle mixtures were injected into inlet A with a flow rate of 0.5–8 μL min^{-1}. The flow rate of inlet B was fixed at 5 μL min^{-1} for all experiments, and the flow rate of inlet C (3.5–7 μL min^{-1}) was adjusted accordingly to make the ferrofluid/buffer boundary just right below outlet 4, to allow for particle and cell extraction. The magnet was placed 1, 4 and 7 mm away from the channel, which corresponded to magnetic field strengths of 300, 134 and 72 mT and magnetic field gradients of 83.4, 32.2 and 12.9 T m^{-1} (ESI,† Fig. S1). Ferrofluid concentrations of 0.13, 0.26 and 0.39% (v/v) were used.

For experiments on separation of cancer cells from cell lines/RBCs and cancer cells from cell lines/WBCs, cell mixtures were injected into inlet A at a flow rate of 20 μL min^{-1}. The magnet was placed 4 mm away from the channel and ferrofluids with a concentration of 0.26% (v/v) were used. After separation, cells from outlet 4 were collected into a 96-well plate for counting under a fluorescence microscope.

Simulation

Cell trajectories were simulated in a three-dimensional (3D) manner by modifying previously developed models with a concentration profile of ferrofluids across the width of the microchannel.[28,29] Briefly, we used an analytical model that could predict the 3D transport of diamagnetic cells in ferrofluids inside a microfluidic channel coupled with permanent magnets (see the ESI†). The magnets produced a spatially non-uniform magnetic field that led to a magnetic buoyancy force on the cells. The resulting trajectories of the cells were obtained by (1) calculating the 3D magnetic buoyancy force *via* an experimentally verified and analytical distribution of magnetic fields as well as their gradients, together with a nonlinear magnetization model of the ferrofluid, (2) deriving the hydrodynamic viscous drag force with an analytical velocity profile in the channel including the "wall effect", and (3) solving governing equations of motion using analytical expressions of the magnetic buoyancy force and hydrodynamic viscous drag force. The parameters of simulation (device dimensions and geometry, fluid and cell properties, and magnetic fields) reflected exact experimental conditions.

Results and discussion

Ferrofluid properties

Fig. 2a shows the size distribution and a sample TEM image of maghemite nanoparticles of the custom-made ferrofluid. The particles had a mean diameter of 11.24 nm with a standard deviation of 2.52 nm. Although nanoparticles with larger diameters were considered to be more biocompatible because they may inhibit direct diffusion across the cell membrane,[30–33] we chose this diameter for the nanoparticles to preserve the colloidal stability of the ferrofluids against agglomeration due to gravitational settling and magnetic dipole–dipole attraction.[15] Particles with a large diameter are

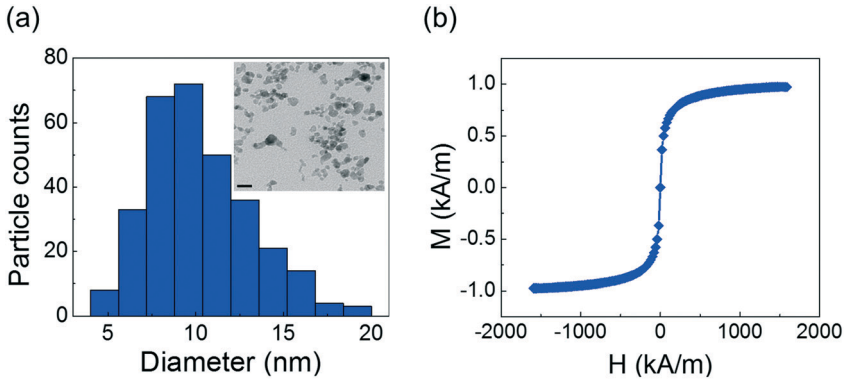

Fig. 2 (a) Size distribution of the maghemite nanoparticles within the ferrofluid (11.24 ± 2.52 nm). Inset: A TEM image of the maghemite nanoparticles in the ferrofluid. Scale bar: 20 nm. (b) Magnetization curve of the ferrofluid. The saturation magnetization of this ferrofluid is 0.96 kA m^{-1}, corresponding to a 0.26% volume fraction of magnetic materials.

prone to settling and agglomeration, and can disrupt continuous-flow separation. However, at a diameter of ~10 nm, thermal agitation at room temperature is sufficient to keep particles separated. As a result, our ferrofluids remained colloidally stable after at least 10 months of storage. The nanoparticles were also functionalized with a graft copolymer as surfactant to prevent them from coming too close to one another when there was a magnetic field. In all of the cell manipulation experiments conducted here, our ferrofluids did not show any sign of nanoparticle agglomeration under magnetic fields. We measured the saturation magnetization of the as-synthesized ferrofluid to be 0.96 kA m^{-1}, as shown in Fig. 2b. Considering that the bulk magnetization of maghemite is about 370 kA m^{-1},[34] we estimated the volume fraction of the magnetic content of the ferrofluid to be 0.26%. The low volume fraction of the ferrofluid not only led to good biocompatibility for live cells but also enabled us to observe cell motion in the microchannel directly with bright-field microscopy, which was difficult with opaque ferrofluids of high solid volume fractions. The surface charge of the particles was negative, measured by a zeta potential of −27.2 ± 11.4 mV (ESI,† Fig. S2). The ferrofluid was made to be

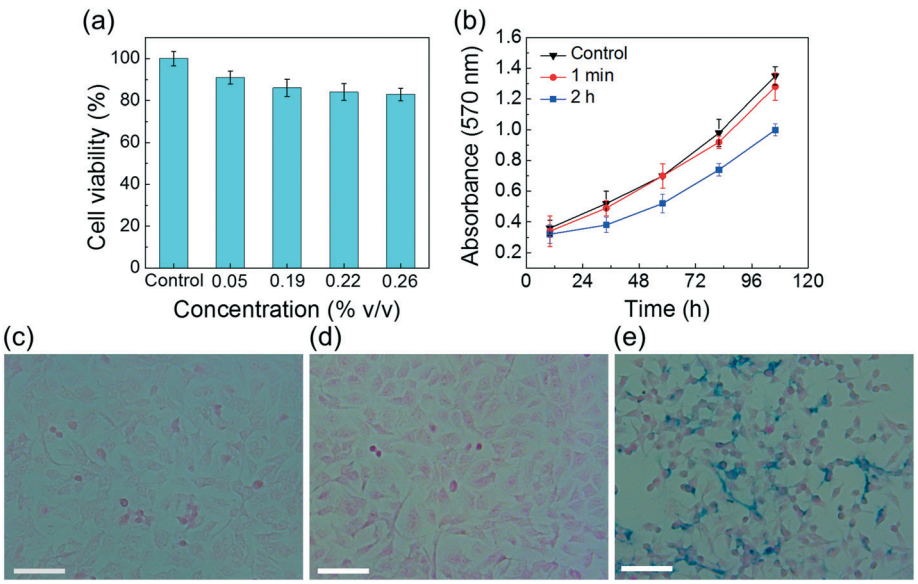

Fig. 3 (a) Cell viability of A549 cells was evaluated by MTT assay. Different concentrations of ferrofluids (0.05%, 0.19%, 0.22%, and 0.26% v/v) were added to the incubation medium. Average cell viabilities were 100% in the control, 91% in 0.05% ferrofluid, 86% in 0.19% ferrofluid, 84% in 0.22% ferrofluid, and 83% in 0.26% ferrofluid, after 12 hours of incubation with ferrofluids. (b) Growth curves of A549 cells with different times of exposure to ferrofluids were determined by MTT assay. The cells incubated with ferrofluids for 2 h grew more slowly than the control group. No significant difference was found between the cells incubated with ferrofluids for 1 min and the control group. (c–e) Cellular nanoparticle uptake of A549 cells. The cells were incubated with ferrofluids for 0, 1 min, and 2 h and then subjected to Prussian blue staining. Positive staining was visible in the majority of the cells that were incubated with ferrofluids for 2 h (e). Incubation with ferrofluids for 1 min showed little cellular uptake of nanoparticles (d). (c) Control. Scale bars: 50 μm.

isotonic and its pH was adjusted to 7.0 for biocompatible cell manipulation.

Ferrofluid biocompatibility

We investigated the biocompatibility of this ferrofluid by exposing a total of 7 cancer cell lines to it and studying their short-term viability, long-term cell proliferation, and cellular nanoparticle uptake after the exposure. These cell lines included two lung cancer cell lines (A549 and H1299), three breast cancer cell lines (HCC1806, MDA-MB-231 and MCF-7), one prostate cancer cell line (PC-3), and one cervical cancer cell line (HeLa). We chose these cell lines because they were frequently used to validate new microfluidic separation technologies for cancer cells.

Short-term cell viability was examined using MTT assay. Here, we used the A549 lung cancer cell line as an example to describe the results. Fig. 3a compares A549 cell viabilities after 12 hours of exposure to a control medium and 4 different concentrations (0.05%, 0.19%, 0.22%, and 0.26% v/v) of custom-made ferrofluids. A549 cells showed 100 ± 3% viability in the control medium and gradually decreasing viabilities in the ferrofluids (91 ± 3% viability for 0.05% ferrofluid, 86 ± 4% viability for 0.19% ferrofluid, 83 ± 4% viability for 0.22% ferrofluid, and 83 ± 3% viability for 0.26% ferrofluid). This is expected as the nanoparticle concentration does affect the short-term cell viability, due to either particle diffusion across the cellular membrane or endocytosis of particles by cells. Still, A549 cells retained 83 ± 3% viability in the 0.26% ferrofluid concentration after a 12 hour period of exposure, which was at least 6 times longer than those in current cell viability studies in custom-made ferrofluids.[3,16,18] Such a long period of exposure is typically not necessary for high-throughput cell separation; a more reasonable estimated time of ferrofluid exposure for current cell separation schemes is 1–2 hours. Within such a time frame, Table 1 summarizes the results for all 7 cell lines, which showed consistently over 90% viability after 2 hours of exposure in the 0.26% ferrofluid. They confirmed that this ferrofluid had minimal detrimental effects on the 7 cancer cell lines in the short term.

In addition to short-term viability, we also examined whether all cell lines were able to proliferate normally after exposure to ferrofluids. As shown in Table 1, all 7 cell lines were capable of normal proliferation to confluence after 2 hours of incubation in the ferrofluid. This is the first time that long-term effects of a colloidally stable ferrofluid were studied on several cancer cell lines. To the best of our knowledge, Yellen's group conducted the only proliferation study using HUVEC after exposure to a bovine serum albumin-coated ferrofluid.[18]

Our ferrofluid showed excellent short-term and long-term biocompatibility for the 7 types of cancer cells. As discussed earlier, even with such a ferrofluid, it is still better to minimize the time of cells' exposure to it, as prolonged exposure time will inevitably lead to particle endocytosis and/or diffusion, which may affect cells' normal functions. To investigate the effect of exposure time on cell proliferation, we examined A549 cells again using both MTT assay for proliferation and Prussian blue assay for nanoparticle uptake. This time, A549 cells were either seeded directly into a 96-well plate as a control or incubated in ferrofluids for 1 minute and 2 hours. Their proliferation measurements (absorbance at 570 nm for MTT assay) were evaluated and recorded every 24 hours, and their nanoparticle uptake (iron distribution) was imaged after incubation with ferrofluids using Prussian blue assay. Fig. 3b compares cell proliferations between the control, 1 minute exposure, and 2 hour exposure to ferrofluids. No significant change was found between the control and 1 minute exposure; cells incubated in ferrofluids for 1 minute were able to proliferate normally and resulted in nearly the same growth rate as the control. This was also confirmed by nanoparticle uptake comparison in Fig. 3c and d, which show the presence of almost identical and little amounts of iron. On the other hand, 2 hour exposure to ferrofluids did affect A549 cell proliferation in a noticeable and negative way, evidenced by a lower growth rate in Fig. 3b and the significant presence of iron in Fig. 3e. The longer time of A549 cells' exposure to ferrofluids led to the higher cellular uptake of nanoparticles and slower cell growth. It is therefore beneficial to minimize the time of cells' exposure to ferrofluids.

Device optimization and calibration

We previously described the general idea behind the device design to significantly decrease the time of cells' exposure to ferrofluids. Briefly, we aimed to eliminate unnecessary exposure time including sample preparation and sample

Table 1 Short-term viability and long-term proliferation of 7 cancer cell lines after exposure to the custom-made biocompatible ferrofluid. Short-term viability was determined by a Live/Dead assay after 2 hours of exposure to the ferrofluid with a 0.26% volume fraction. Long-term proliferation was determined by culturing cells after the same exposure to the ferrofluid

Cell line	A549 (lung cancer)	H1299 (lung cancer)	HeLa (cervical cancer)	MDA-MB-231 (breast cancer)	HCC1806 (breast cancer)	MCF-7 (breast cancer)	PC-3 (prostate cancer)
Viability after 2 hours of exposure to ferrofluids	94%	95%	92%	95%	94%	95%	96%
Proliferation to confluence after 2 hours of exposure to ferrofluids	Yes	Yes	Yes	Yes	Yes	Yes	Yes

extraction and allow cells to be in contact with ferrofluids when it was absolutely necessary (*e.g.*, separation). The flow rate and channel length determined the exposure time in a typical cell separation protocol, which was estimated to be on the order of seconds in our devices. Here, we described the results of device optimization and calibration using analytical

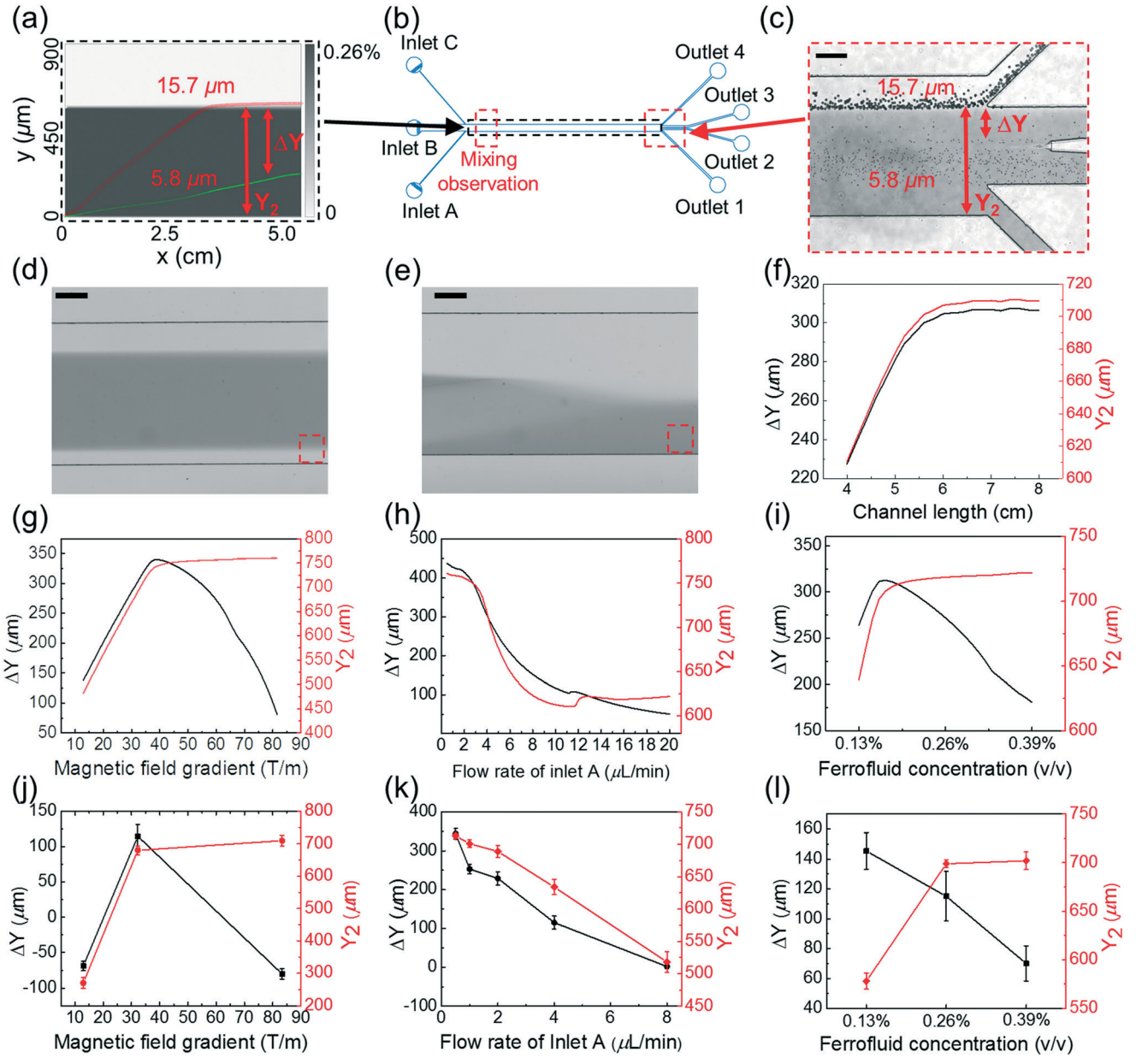

Fig. 4 Device optimization *via* simulations and calibrations. (a) Simulated concentration profile of ferrofluids and the cells' trajectories across ferrofluids and the buffer stream. The ferrofluid concentration is represented by gray scale. The trajectories of a cancer cell with 15.7 μm diameter are indicated by red circles, and the trajectories of a red blood cell with 5.8 μm diameter are indicated by green circles. (b) Schematic of the microchannel with various simulation and observation windows. (c) A representative image of microparticle separation observed in the window from (b). Representative images of magnetic convective mixing (without microparticles) from the observation window in (b) without the magnet (d) and with the magnet (e). The observation window is 6.7 mm away from the entrance of the main channel. The gray scale intensity profile of the red dashed boxes in (d) and (e) can be found in the ESI† (Fig. S3). The flow rate of inlet A is fixed at 4 μL min^{-1}, the ferrofluid concentration is fixed at 0.26%, and the magnetic field gradient is fixed at 32.2 T m^{-1} for (a)–(f). Numerical simulation of separation distance ΔY and deflection distance Y_2 at the end of the channel with parameters including: (f) channel length, (g) magnetic field gradient, (h) flow rate of inlet A, and (i) ferrofluid concentration. Experimental calibration of these parameters for separation distance ΔY and deflection distance Y_2 using microparticles: (j) ΔY and Y_2 as a function of magnetic field gradient, (k) ΔY and Y_2 as a function of flow rate of inlet A, and (l) ΔY and Y_2 as a function of ferrofluid concentration. The flow rate of inlet A is fixed at 4 μL min^{-1} and the ferrofluid concentration is fixed at 0.26% (v/v) for (g) and (j). The magnetic field gradient is fixed at 32.2 T m^{-1} and the ferrofluid concentration is fixed at 0.26% (v/v) for (h) and (k). The magnetic field gradient is fixed at 32.2 T m^{-1} and the flow rate of inlet A is fixed at 4 μL min^{-1} for (i) and (l). Scale bars: 200 μm.

models and microparticles. This optimization was also verified through a separation experiment involving cancer cells from cell culture lines and red blood cells.

We used the 3D analytical model to optimize our device (Fig. 1d) for a potential cell separation application. In this case, we allowed two groups of cells with different sizes to enter the channel and simulated their trajectories. Sample simulated trajectories of the two types of cells (cancer cells with a presumed 15.7 μm diameter and red blood cells with a presumed 5.8 μm diameter) are shown in Fig. 4a. The location of the simulation window is depicted in Fig. 4b. We chose these two cell sizes for simulation because microparticles with exact sizes were available for calibration purposes. From these trajectories, we calculated two outputs – a deflection in the *y*-direction for the larger cancer cells, denoted as Y_2, and a separation distance between the two types of cells, denoted as ΔY. Both outputs were optimized using parameters including channel length (4–8 cm), magnetic fields and gradients (field: 72–300 mT; gradient: 12.9–83.4 T m^{-1}), flow rates of the cell inlet (inlet A in Fig. 1c, 0.5–20 μL min^{-1}), and ferrofluid concentrations (0.13–0.39% v/v). The goal was to achieve separation of larger cancer cells from smaller blood cells, which translated to maximizing both Y_2 and ΔY simultaneously. Calibration of the device used two types of microparticles with diameters of 5.8 μm and 15.7 μm. Experimental conditions for the calibration including magnetic fields, flow rates, and ferrofluid concentrations were the same as those in the simulation. A sample image of the microparticles' trajectories at the outlets is shown in Fig. 4c. We extracted both outputs (Y_2 and ΔY) from the images and used them to compare simulation and calibration results. The location of the experimental observation window is depicted in Fig. 4b. In this device design, cell samples from inlet A were quickly mixed with ferrofluids from inlet B because of strong magnetic convection resulting from interactions between the ferrofluids and permanent magnet.[24,25,35] With typical device and flow parameters used in cell separation, we estimated that homogeneous mixing could be achieved at a channel length of a few millimeters away from the inlets (ESI,† Fig. S3), which was confirmed by experimental observations in Fig. 4d and e. Given that the total channel length was ~5 cm, we considered the effects from mixing on cell separation to be minimal and neglected them in the following optimization.

We first optimized the channel length, as the dimensions of the permanent magnet used in the separation remained constant. Fig. 4f shows that, under typical device and flow parameters, both ΔY and Y_2 increased with the channel length and reached saturation when the length was around 5.8 cm. It should be noted that the optimized channel length could be affected by parameters including flow rates, magnet properties, ferrofluid properties, and cell types. The second set of parameters that we optimized for the device were the magnetic field strength and its gradient, both of which changed values as we adjusted the distance between the magnet and channel (ESI,† Fig. S1). Fig. 4g and j show that, in both simulation and calibration, when the magnetic field gradient increased, the overall deflection Y_2 of 15.7 μm microparticles increased, too. This was because the driving force – magnetic buoyancy force on the microparticles – was determined in part by the gradient. The larger the gradient, the larger the magnetic force and resulting deflection of microparticles. Interestingly, the simulated separation distance between two microparticles ΔY had a peak at a medium gradient (38.2 T m^{-1}), which was confirmed by the calibration experiments. This was due to the fact that both microparticles reached their maximum deflections very quickly under a strong gradient (83.4 T m^{-1}) in the device, resulting in mixing rather than separation of the two types of microparticles. On the other hand, the separation distance also decreased when the gradient was too weak (12.9 T m^{-1}) to deflect the microparticles and distinguish them. As a result, we chose to use the medium field and gradient (134 mT and 32.2 T m^{-1}) for subsequent cell separation.

A third parameter to optimize was the flow rate of the cell inlet (inlet A in Fig. 1c). Both simulation (Fig. 4h) and calibration (Fig. 4k) results show a monotonically decreasing trend for Y_2 and ΔY as the magnitude of the flow rate increased. This was consistent with the findings from existing cell separation technologies,[36] where a tradeoff existed between throughput (flow rate in this case) and separation efficiency (separation distance ΔY in this case).

The last parameter that we chose to optimize was the ferrofluid concentration. Generally speaking, a higher concentration of ferrofluid resulted in a higher magnitude of magnetic force on the microparticles, leading to a larger deflection, which was observed in both simulation and calibration (Fig. 4i and l) of Y_2. However, a high ferrofluid concentration was not necessarily beneficial for achieving a larger separation distance ΔY. Fig. 4i shows that there was an optimal ferrofluid concentration close to 0.17% (v/v) for both ΔY and Y_2. Concentrations higher than 0.17% (v/v) resulted in larger Y_2 but smaller ΔY. This was because both microparticles achieved sufficient deflections in a strongly magnetized ferrofluid, resulting in mixing rather than separation of the two. Microparticle calibration experiments, as shown in Fig. 4l, did not capture this optimal concentration, as there were only three concentrations of ferrofluids used.

While the simulation and calibration results matched each other quite well qualitatively, we noticed quantitative differences between the two for the separation distance ΔY. The simulation consistently yielded larger ΔY than the calibration. This might be due to the fact that the simulation did not take into account the widening of cell streams, which effectively reduced the separation distance, as shown in Fig. 4c.

Because of the device design and the diffusion between the ferrofluids and buffer stream, the cell separation efficiency and the amount of ferrofluids in the collection outlet could affect each other. In this study, our goal was to not only achieve biocompatible and label-free cell separation with the best possible separation efficiency, but also maintain cell integrity. As a result, we optimized the flow rates of the

ferrofluids and buffer stream so that their diffusion boundary was at exactly the boundary of outlet 3 and outlet 4 (collection outlet). This way, the majority of spiked cancer cells could be extracted, while the amount of ferrofluids was minimized in the collection outlet. We estimated the concentration of magnetic nanoparticles that diffused into the collection outlet to be ~0.002% (v/v) *via* a simulation using typical flow rate parameters. A magnetization measurement from one experiment revealed a 0.00128% (v/v) concentration (ESI,† Fig. S4) of the liquid collected from the same outlet, which was on the same order of magnitude as that from the simulation. This measured concentration of nanoparticles in the collection outlet was 203-fold more dilute than the original ferrofluid, and unlikely induced detrimental effects to cells. We also estimated *via* a simulation the overall time of cells' exposure to ferrofluids to be 4–53 seconds depending on the cell input flow rates (0.5–20 μL min^{-1}) in the current devices.

Finally, we verified these optimized and calibrated parameters (magnetic field and gradient: 134 mT and 32.2 T m^{-1}, ferrofluid concentration: 0.26% v/v, channel length: 5.8 cm) with separation of spiked cancer cells (A549 lung cancer and MCF-7 breast cancer, 100 cells per mL) from diluted human whole blood (RBC concentration: 2×10^6 cells per mL) at 0.9 mL h^{-1} throughput. Detailed results are summarized in the ESI† (Fig. S5 and Table S1). Briefly, the separation efficiency (defined as the ratio of captured cancer cells to spiked cancer cells) for the A549 cell line was 77 ± 6%, and the purity of cancer cells recovered (defined as the ratio of cancer cells to all cell types in the collection outlet) was 62.1 ± 0.9%. The separation efficiency for the MCF-7 cell line was 84 ± 4%, and its purity was 59.2 ± 0.8%. We concluded that these optimized parameters could be used to enable high-throughput and high-efficiency low-concentration cell separation in ferrofluids.

Cell separation

We chose to validate the biocompatible cell separation strategy using spiked cancer cells from cell culture lines in undiluted white blood cells (WBCs). Separating spiked cancer cells from WBCs is potentially the first step to render ferrofluid-based "negative magnetophoresis" useful in rare cell separation applications such as enrichment of circulating tumor cells (CTCs) from peripheral blood.[1] Since CTCs occur at an extremely low concentration of 1–10 cells every 1 billion RBCs and 1 million of WBCs,[37–39] their enrichment requires the development of highly efficient and high-throughput separation.[21] For this purpose, we scaled up the device by increasing the depth of the device from 52 μm to 150 μm in Fig. 1d to accommodate high cell flow rates (20 μL min^{-1}, *i.e.*, 1.2 mL h^{-1}, see ESI† Fig. S6 for device calibration) and chose the optimized magnetic field and gradient (134 mT and 32.2 T m^{-1}), ferrofluid concentration (0.26% v/v), and channel length (5.8 cm) based on previous optimization and calibration results. The mean diameters of all cells used here were measured to be 15.5 μm for A549, 16.9 μm for H1299, 18.7 μm for MCF-7, 18.1 μm for MDA-MB-231, 18.9 μm for PC-3, and 11.1 μm for WBCs.

We validated the separation of spiked cancer cells from undiluted human blood with only WBCs. This is more challenging than separating cancer cells and RBCs, as the size differences between cancer cells and WBCs are much more subtle. We used A549, H1299, MCF-7, MDA-MB-231, and PC-3 cell lines, with a spike ratio of ~100 cells in 1 mL of undiluted WBCs. The cell flow rate was 1.2 mL h^{-1}. Experimental results are summarized in Fig. 5a–c and Table 2. Fig. 5a shows that A549 cancer cells and WBCs flowed near the bottom of the channel and exited through outlet 1, resulting in no separation of the two when there was no magnetic field. Fig. 5b shows that larger A549 cancer cells deflected from the ferrofluid stream into the PBS buffer stream toward outlet 4 when there was a magnetic field. WBCs remained in the ferrofluid stream and exited through outlets 2 and 3. The fluorescence image of A549 cells in Fig. 5c confirmed such separation. From Table 2, the separation efficiency for A549 cells was 80 ± 3%. The purity of cancer cells was 25.3 ± 0.1% from outlet 4. Similar experiments were carried out to separate multiple cancer cell lines from WBCs. The separation efficiencies were 81 ± 5%, 82 ± 5%, 82 ± 4%, and 86 ± 6% for H1299, MCF-7, MDA-MB-231, and PC-3 cells. Even with the subtle size difference between the cancer cells and WBCs, we were able to achieve high separation efficiency (80–86%) using this strategy. The purity of cancer cells was on the order of 20% for all cases. This size-based separation strategy performed well in separating cancer cells from WBCs. As the diameter of cancer cells increased from 15.5 μm (A549) to 18.9 μm (PC-3), we observed a slight increase in separation efficiency, which is expected as the separation is based on size difference of cell types.

We investigated the short-term viability and long-term proliferation of separated A549 cancer cells collected from the device. After running the cell mixture through the device for separation, A549 cells were collected from outlet 4 and studied for their viability using a Live/Dead assay. Fig. 6a shows that the viability of A549 cells before and after separation was 95.2 ± 2.0% and 93.8 ± 1.5%, respectively. Fig. 6b shows representative fluorescence images of A549 cells before and after separation using a Live/Dead stain. They indicate no significant impact from ferrofluid exposure and cell processing on cell viability. We also examined the long-term proliferation of A549 cancer cells after separation. Fig. 6c shows the images of A549 cells over a 4 day period and Live/Dead staining of the cultured cells on day 4. We concluded that A549 cells were able to proliferate to confluence.

In summary, we developed a biocompatible and label-free cell separation method using ferrofluids, to differentiate between low-concentration cancer cells from cell culture lines and WBCs with subtle size differences in a high-throughput and high-efficiency manner. Separated cancer cells showed

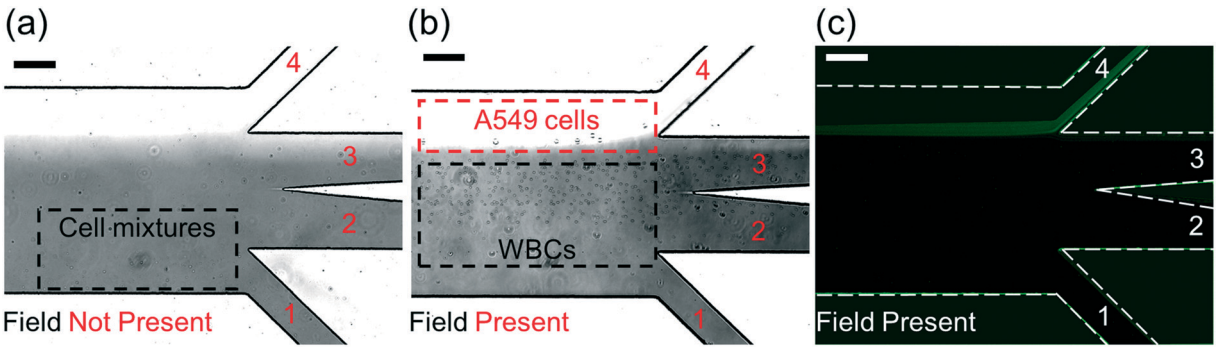

Fig. 5 Micrographs of separation processes of spiked cancer cells from cell culture lines and white blood cells (WBCs). (a) In the absence of magnetic fields, cell mixtures exited the channel through outlet 1. (b) When magnetic fields were present, larger A549 cancer cells were deflected and reached the ferrofluid/buffer boundary, then exited through outlet 4 (collection outlet), while smaller WBCs exited through other outlets. (c) Fluorescence image of A549 cancer cells during cell separation. A549 cells were stained with CellTracker Green. Dashed white lines depict the microchannel boundaries. Scale bars: 200 μm.

Table 2 Summary of cancer cell separation performance

Cell line	No. of cells spiked	No. of cells captured	Efficiency	No. of WBCs	Purity
A549	100	80 ± 3	80 ± 3%	236 ± 22	25.3 ± 0.1%
H1299	100	81 ± 5	81 ± 5%	218 ± 15	27.1 ± 0.1%
MCF-7	100	82 ± 5	82 ± 5%	208 ± 29	28.3 ± 0.1%
MDA-MB-231	100	82 ± 4	82 ± 4%	233 ± 48	26.0 ± 0.2%
PC-3	100	86 ± 6	86 ± 6%	212 ± 32	28.8 ± 0.1%

100 CellTracker Green-stained cancer cells were spiked into 1 mL of WBCs. Data are expressed as mean ± S.D., n = 3.

excellent average viability (94.4 ± 1.3%) and normal proliferation. This could be useful in preserving cell integrity for further analysis after enrichment. We achieved on average 82.2% separation efficiency in separating a variety of cancer cells from cell culture lines from WBCs at an extremely low concentration of ∽100 cells per mL with a throughput of 1.2 mL h^{-1}. The efficiency obtained here is comparable to the average reported efficiency of 82% from recent label-free microfluidic separation of cultured cancer cells in blood.[21] For example, the separation efficiency reported here is close to the efficiencies of methods based on standing surface acoustic waves,[40] dielectrophoresis,[41–43] and slanted spiral channels,[44] and is higher than the efficiency of vortex technology.[45–47] The purity of recovered cancer cells from this method was between 25.3% and 28.8% depending on specific cell lines. It is also comparable to the reported purity values from existing label-free methods when they were used to separate spiked cancer cells from blood. These reported purities varied dramatically from 0.1% to 90%,[40–47] as most of the label-free methods focused on improving the separation efficiency of low-concentration cells, rather than their purity. For example, the recovered cancer cell purity of this method is higher than the purities reported from the standing surface acoustic wave method (0.1%, calculated from ∼90% WBC removal rate after separation)[40] and a few dielectrophoretic methods (10% (ref. 42) and 16.24% (ref. 43)), but lower than the purities from the slanted spiral channel method (50%)[44] and the vortex technology (57–94%).[45–47]

Although the throughput of the current devices (1.2 mL h^{-1}) is comparable to the throughput from methods based on standing surface acoustic waves[40] and dielectrophoresis,[41–43] it needs improvement in order to handle a clinically relevant amount of human blood (*e.g.*, 7.5 mL h^{-1} for enrichment of CTCs), which was demonstrated by methods such as slanted spiral channel[44] and vortex technology.[45–47] Further scale-up of a single device and/or potential multiplexing of several devices together could improve the throughput. As a proof-of-concept demonstration, this method was used to separate low-concentration spiked cancer cells from WBCs, with the RBCs removed beforehand using a RBC lysis buffer. In the future, it is beneficial and necessary to design a two-step separation device, which can first remove the bulk of RBCs, and then further enrich cancer cells from mostly WBCs to automate whole blood processing on-chip. While other methods have been demonstrated to be able to handle clinical samples such as whole blood,[40,43–47] this method was still at its early stage of development and was limited to cultured cancer cells. Future studies using whole blood need to be conducted to further evaluate the potential of this method in rare cell separation.

Conclusions

In this study, we reported a biocompatible and label-free method for separation of low-concentration cancer cells from cell culture lines from undiluted white blood cells based on their size difference, by using a custom-made ferrofluid and

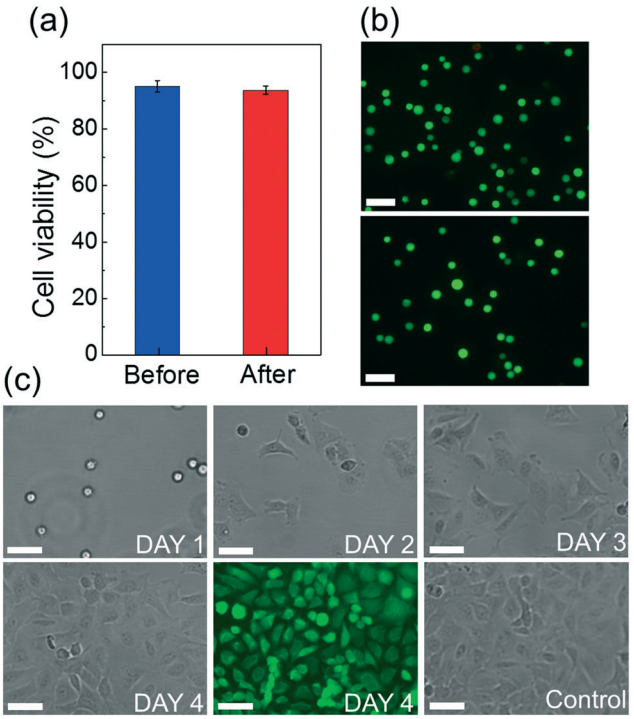

Fig. 6 (a) Short-term cell viability comparison between before *vs.* after separation groups. No significant difference was found between the two. (b) Representative images of Live/Dead staining of the before (top) and after separation (bottom) groups. Calcein-AM (green) and PI (red) channels were merged in these images. Scale bars: 100 μm. (c) Bright-field images of cultured A549 cells collected after separation from day 1 to day 4. Live/Dead staining of the cultured cells on day 4 showed excellent viability. A control group of cell culture was used for comparison. No significant difference was found in cell proliferation between cells in the control group and cells collected after device separation. Scale bars: 50 μm.

integrating on-chip sample preparation, separation and extraction into a microfluidic device. The ferrofluid possessed not only ideal biocompatible properties for live cell manipulation, including its low magnetic content (*e.g.*, 0.26% volume fraction), neutral pH, isotonicity, maghemite nanoparticles and their surfactant but also excellent colloidal stability that enables high-throughput and high-efficiency continuous separation. A biocompatibility study of 7 commonly used cancer cell lines showed consistently over 90% short-term viabilities and abilities to proliferate to confluence for all cells, even after extended exposure to this ferrofluid. Additionally, an optimized device design eliminated time-consuming off-chip sample preparation and extraction steps, which reduced the overall time of cells' exposure to ferrofluids from hours to seconds. To demonstrate the potential of this method in rare cell separation, a variety of cancer cells from cell culture lines in white blood cells were separated with an average efficiency of 82.2%, at a throughput of 1.2 mL h^{-1} with an extremely low concentration of ~100 cancer cells per mL. Separated cancer cells showed excellent viability and normal proliferation. This method addressed the challenges associated with cell separation in ferrofluids, including excellent biocompatibility of not only the custom-made ferrofluid but also the assay itself, as well as device design and optimization specifically for the low concentration of target cells. While still at its early stage of development, this method could be a promising tool for rare cell separation because of its excellent biocompatibility, label-free operation, and performance with cultured cancer cells, along with potential for device scale-up, multiplexing, and further optimization.

Acknowledgements

We thank Ms. Nneoma E. Okonkwo (a National Science Foundation funded REU student) for her help in the initial calibration of the technology. This study is supported by the National Science Foundation under Grant No. 1150042, 1242030, and 1359095 and by the National Institute of General Medical Sciences of the National Institutes of Health under Award No. R21GM104528. The content is solely the responsibility of the authors and does not necessarily represent the official views of the National Institutes of Health.

References

1 W. Zhao, R. Cheng, J. R. Miller and L. Mao, *Adv. Funct. Mater.*, 2016, **26**, 3916–3932.
2 F. Shen, H. Hwang, Y. K. Hahn and J. K. Park, *Anal. Chem.*, 2012, **84**, 3075–3081.
3 A. R. Kose, B. Fischer, L. Mao and H. Koser, *Proc. Natl. Acad. Sci. U. S. A.*, 2009, **106**, 21478–21483.
4 J. Zeng, Y. X. Deng, P. Vedantam, T. R. Tzeng and X. C. Xuan, *J. Magn. Magn. Mater.*, 2013, **346**, 118–123.
5 A. Winkleman, K. L. Gudiksen, D. Ryan, G. M. Whitesides, D. Greenfield and M. Prentiss, *Appl. Phys. Lett.*, 2004, **85**, 2411–2413.
6 A. I. Rodriguez-Villarreal, M. D. Tarn, L. A. Madden, J. B. Lutz, J. Greenman, J. Samitier and N. Pamme, *Lab Chip*, 2011, **11**, 1240–1248.
7 J. Zeng, C. Chen, P. Vedantam, T. R. Tzeng and X. C. Xuan, *Microfluid. Nanofluid.*, 2013, **15**, 49–55.
8 P. Kauffmann, A. Ith, D. O'Brien, V. Gaude, F. Boue, S. Combe, F. Bruckert, B. Schaack, N. M. Dempsey, V. Haguet and G. Reyne, *Lab Chip*, 2011, **11**, 3153–3161.
9 N. G. Durmus, C. Tekin, S. Guven, K. Sridhar, A. A. Yildiz, G. Calibasi, I. Ghiran, R. W. Davis, L. M. Steinmetz and U. Demirci, *Proc. Natl. Acad. Sci. U. S. A.*, 2015, **112**, 3661–3668.
10 S. Tasoglu, J. A. Khoory, H. C. Tekin, C. Thomas, A. E. Karnoub, I. C. Ghiran and U. Demirci, *Adv. Mater.*, 2015, **27**, 3901–3908.
11 S. Knowlton, C. H. Yu, N. Jain, I. C. Ghiran and S. Tasoglu, *PLoS One*, 2015, **10**, e0134400.
12 B. Yenilmez, S. Knowlton and S. Tasoglu, *Adv. Mater. Technol.*, 2016, **1**, 1600144–1600153.
13 S. M. Knowlton, I. Sencan, Y. Aytar, J. Khoory, M. M. Heeney, I. C. Ghiran and S. Tasoglu, *Sci. Rep.*, 2015, **5**, 15022.
14 A. T. Skjeltorp, *Phys. Rev. Lett.*, 1983, **51**, 2306–2309.
15 R. E. Rosensweig, *Ferrohydrodynamics*, Cambridge University Press, Cambridge, UK, 1985.

16 W. Zhao, T. Zhu, R. Cheng, Y. Liu, J. He, H. Qiu, L. Wang, T. Nagy, T. D. Querec, E. R. Unger and L. Mao, *Adv. Funct. Mater.*, 2016, **26**, 3990–3998.
17 U. Dharmasiri, M. A. Witek, A. A. Adams and S. A. Soper, *Annu. Rev. Anal. Chem.*, 2010, **3**, 409–431.
18 M. D. Krebs, R. M. Erb, B. B. Yellen, B. Samanta, A. Bajaj, V. M. Rotello and E. Alsberg, *Nano Lett.*, 2009, **9**, 1812–1817.
19 S. D. Conner and S. L. Schmid, *Nature*, 2003, **422**, 37–44.
20 T. T. Zhu, R. Cheng, S. A. Lee, E. Rajaraman, M. A. Eiteman, T. D. Querec, E. R. Unger and L. D. Mao, *Microfluid. Nanofluid.*, 2012, **13**, 645–654.
21 Y. C. Chen, P. Li, P. H. Huang, Y. L. Xie, J. D. Mai, L. Wang, N. T. Nguyen and T. J. Huang, *Lab Chip*, 2014, **14**, 626–645.
22 G. P. Zhu, M. Hejiazan, X. Y. Huang and N. T. Nguyen, *Lab Chip*, 2014, **14**, 4609–4615.
23 M. D. Tarn, M. J. Lopez-Martinez and N. Pamme, *Anal. Bioanal. Chem.*, 2014, **406**, 139–161.
24 M. Hejazian, D. T. Phan and N. T. Nguyen, *RSC Adv.*, 2016, **6**, 62439–62444.
25 M. Hejazian and N.-T. Nguyen, *Micromachines*, 2017, **8**, 37.
26 R. Massart, *IEEE Trans. Magn.*, 1981, **17**, 1247–1248.
27 Y. N. Xia and G. M. Whitesides, *Annu. Rev. Mater. Sci.*, 1998, **28**, 153–184.
28 R. Cheng, T. T. Zhu and L. D. Mao, *Microfluid. Nanofluid.*, 2014, **16**, 1143–1154.
29 T. T. Zhu, D. J. Lichlyter, M. A. Haidekker and L. D. Mao, *Microfluid. Nanofluid.*, 2011, **10**, 1233–1245.
30 J. Huang, L. H. Bu, J. Xie, K. Chen, Z. Cheng, X. G. Li and X. Y. Chen, *ACS Nano*, 2010, **4**, 7151–7160.
31 N. Luciani, F. Gazeau and C. Wilhelm, *J. Mater. Chem.*, 2009, **19**, 6373–6380.
32 D. L. J. Thorek and A. Tsourkas, *Biomaterials*, 2008, **29**, 3583–3590.
33 W. Jiang, B. Y. S. Kim, J. T. Rutka and W. C. W. Chan, *Nat. Nanotechnol.*, 2008, **3**, 145–150.
34 D. K. Hwang, D. Dendukuri and P. S. Doyle, *Lab Chip*, 2008, **8**, 1640–1647.
35 L. Mao and H. Koser, OVERCOMING THE DIFFUSION BARRIER: ULTRA-FAST MICRO-SCALE MIXING VIA FERROFLUIDS, *The 14th International Conference on Solid-State Sensors, Actuators and Microsystems, 2007*, June 10-14, 2007, Lyon, France.
36 D. R. Gossett, W. M. Weaver, A. J. Mach, S. C. Hur, H. T. K. Tse, W. Lee, H. Amini and D. Di Carlo, *Anal. Bioanal. Chem.*, 2010, **397**, 3249–3267.
37 C. Alix-Panabieres and K. Pantel, *Clin. Chem.*, 2013, **59**, 110–118.
38 C. Alix-Panabieres and K. Pantel, *Nat. Rev. Cancer*, 2014, **14**, 623–631.
39 M. Yu, S. Stott, M. Toner, S. Maheswaran and D. A. Haber, *J. Cell Biol.*, 2011, **192**, 373–382.
40 P. Li, Z. M. Mao, Z. L. Peng, L. L. Zhou, Y. C. Chen, P. H. Huang, C. I. Truica, J. J. Drabick, W. S. El-Deiry, M. Dao, S. Suresh and T. J. Huang, *Proc. Natl. Acad. Sci. U. S. A.*, 2015, **112**, 4970–4975.
41 S. B. Huang, M. H. Wu, Y. H. Lin, C. H. Hsieh, C. L. Yang, H. C. Lin, C. P. Tseng and G. B. Lee, *Lab Chip*, 2013, **13**, 1371–1383.
42 P. R. C. Gascoyne, J. Noshari, T. J. Anderson and F. F. Becker, *Electrophoresis*, 2009, **30**, 1388–1398.
43 H. S. Moon, K. Kwon, S. I. Kim, H. Han, J. Sohn, S. Lee and H. I. Jung, *Lab Chip*, 2011, **11**, 1118–1125.
44 M. E. Warkiani, G. F. Guan, K. B. Luan, W. C. Lee, A. A. S. Bhagat, P. K. Chaudhuri, D. S. W. Tan, W. T. Lim, S. C. Lee, P. C. Y. Chen, C. T. Lim and J. Han, *Lab Chip*, 2014, **14**, 128–137.
45 J. Che, V. Yu, M. Dhar, C. Renier, M. Matsumoto, K. Heirich, E. B. Garon, J. Goldman, J. Y. Rao, G. W. Sledge, M. D. Pegram, S. Sheth, S. S. Jeffrey, R. P. Kulkarni, E. Sollier and D. Di Carlo, *Oncotarget*, 2016, **7**, 12748–12760.
46 M. Dhar, E. Pao, C. Renier, D. E. Go, J. Che, R. Montoya, R. Conrad, M. Matsumoto, K. Heirich, M. Triboulet, J. Y. Rao, S. S. Jeffrey, E. B. Garon, J. Goldman, N. P. Rao, R. Kulkarni, E. Sollier-Christen and D. Di Carlo, *Sci. Rep.*, 2016, **6**, 35474.
47 E. Sollier, D. E. Go, J. Che, D. R. Gossett, S. O'Byrne, W. M. Weaver, N. Kummer, M. Rettig, J. Goldman, N. Nickols, S. McCloskey, R. P. Kulkarni and D. Di Carlo, *Lab Chip*, 2014, **14**, 63–77.